Chaotic dynamics from coupled magnetic monodomain and Josephson current

A. E. Botha [1], Yu. M. Shukrinov [2,3,4], J. Tekić [5], and M. R. Kolahchi [6]

[1]*Department of Physics, University of South Africa, Private Bag X6, Roodepoort, Johannesburg 1710, South Africa*
[2]*BLTP, JINR, Dubna, Moscow Region 141980, Russian Federation*
[3]*Department of Nanotechnology and New Materials, Dubna State University, Dubna, Moscow Region 141980, Russian Federation*
[4]*Moscow Institute of Physics and Technology (National Research University), Institutskii per. 9, 141701 Dolgoprudny, Moscow Region, Russian Federation*
[5]*Laboratory for Theoretical and Condensed Matter Physics-020, "Vinča" Institute of Nuclear Sciences, National Institute of the Republic of Serbia, University of Belgrade, P.O. Box 522, 11001 Belgrade, Republic of Serbia*
[6]*Department of Physics, Institute for Advanced Studies in Basic Sciences, Zanjan 45137-66731, Iran*

(Received 19 November 2022; accepted 27 January 2023; published 10 February 2023)

The ordinary (superconductor-insulator-superconductor) Josephson junction cannot exhibit chaos in the absence of an external ac drive, whereas in the superconductor-ferromagnet-superconductor Josephson junction, known as the φ_0 junction, the magnetic layer effectively provides two extra degrees of freedom that can facilitate chaotic dynamics in the resulting four-dimensional autonomous system. In this work, we use the Landau-Lifshitz-Gilbert model for the magnetic moment of the ferromagnetic weak link, while the Josephson junction is described by the resistively capacitively shunted-junction model. We study the chaotic dynamics of the system for parameters surrounding the ferromagnetic resonance region, i.e., for which the Josephson frequency is reasonably close to the ferromagnetic frequency. We show that, due to the conservation of magnetic moment magnitude, two of the numerically computed full spectrum Lyapunov characteristic exponents are trivially zero. One-parameter bifurcation diagrams are used to investigate various transitions that occur between quasiperiodic, chaotic, and regular regions as the dc-bias current through the junction, I, is varied. We also compute two-dimensional bifurcation diagrams, which are similar to traditional isospike diagrams, to display the different periodicities and synchronization properties in the I-G parameter space, where G is the ratio between the Josephson energy and the magnetic anisotropy energy. We find that as I is reduced the onset of chaos occurs shortly before the transition to the superconducting state. This onset of chaos is signaled by a rapid rise in supercurrent ($I_S \longrightarrow I$) which corresponds, dynamically, to increasing anharmonicity in phase rotations of the junction.

DOI: 10.1103/PhysRevE.107.024205

I. INTRODUCTION

With the view of facilitating new developments in computer technologies, superconducting spintronics has become, recently and most likely for the foreseeable future, an active area of scientific research [1–6]. Since the original work by Buzdin [7], it is known that a significant interaction can occur between the superconducting current and the magnetic moment of the ferromagnet forming the weak link in the superconductor-ferromagnet-superconductor Josephson junction. As pointed out in Ref. [1], for example, this "... marriage between superconductivity and ferromagnetism," opens the door for the development of ultrafast spintronic-logic devices and motivates studies of structures with a superconductor-ferromagnet interface [3]. One specific structure that is currently attracting our attention is the superconductor-ferromagnet-superconductor (SFS) Josephson junction (JJ), or more precisely, the SFS φ_0 Josephson junction.

The SFS φ_0 JJ belongs to a special class of anomalous Josephson junctions in which the ferromagnetic layer is noncentrosymmetric and there is broken time-reversal symmetry. In this case, the spin-orbit coupling leads to a phase shift, φ_0, proportional to the magnetic moment perpendicular to the gradient of the asymmetric spin-orbit potential. The resulting current-phase relation is $I = I_c \sin(\varphi - \varphi_0)$ [7]. Such direct coupling, between the phase difference of superconductors and the magnetic moment of the barrier, provides opportunities to control the magnetic moment via the Josephson current [8], and vice versa, i.e., to influence the Josephson current via the magnetic moment [9]. The φ_0 phase shift permits the magnetic moment to "pump" a dc component of a supercurrent through the junction, which provides a new route to amplify a supercurrent using the magnetization precession [9]. The validity and significance of the anomalous Josephson junctions with phase shift for spintronic technologies have been confirmed in several recent experiments [10–12].

Josephson junctions can exhibit a wide variety of nonlinear phenomena, including various bifurcations [13] and chaos [14–16]. In the past, chaos control, and chaotic synchronization in Josephson junction arrays and shunted models attracted much attention due to their perspective as high precision voltage standards, high power coherent terahertz sources, and radiation detectors [17–25]. In particular, Basler *et al.* [17] reported on the theory of phase locking and self-

synchronization in a small JJ cell by using the resistively shunted junction (RSJ) model and Hassel *et al.* [18] studied self-synchronization in distributed Josephson junction arrays. Features of spatiotemporal chaos in JJ arrays composed of RSJs were numerically investigated by Bhagavatula *et al.* [19]. Chaos and synchronization in JJs globally coupled by a common resistance were studied in Refs. [20,21]. In Ref. [22], it was shown that chaos and hyperchaos states could coexist in an array of two shunted JJs, independently of whether or not the original states of the junctions were chaotic. Resonance-type chaos related to the parametric resonance in a coupled system of JJs was demonstrated in Refs. [26,27]. In the rf-current-driven JJs, it was found that the amplitude of the rf current played a key role in the development of chaos [14,28–30]. More recently, the importance of chaos in intrinsic JJs and its effects on the current-voltage characteristics (CVCs) and the Shapiro steps were stressed in Refs. [31,32]. A detailed description of the results of chaos studies in a separate JJ and a system of coupled JJs is presented in Refs. [26,27,33].

Chaos in current-driven magnetization oscillators has previously been studied in connection with, for example, spin-wave systems [34], spin-valve oscillators [35], and magnetic nanoparticles [36–39]. However, contrary to all the aforementioned studies, chaos has not yet been studied in the SFS φ_0 JJs, despite their significance for technological applications.

In the present work, we examine the appearance of chaos along the CVC in the SFS φ_0 Josephson junction. This system is composed of a single JJ with a ferromagnetic weak link, which leads to coupling between the magnetic moment and the Josephson current. It is important to note that neither the magnetic moment nor the JJ subsystem is capable of chaos on its own. Each subsystem requires some form of time-dependent excitation to induce chaos. However, here in the coupled system, chaos can occur without any time-dependent drive. Thus, the occurrence of chaos in the coupled system is fundamentally different from previous studies of either driven magnetic moments [36–39] or driven Josephson junctions [14,33,40], separately. In the φ_0 Josephson junction the supercurrent in the junction drives the magnetic moment while, simultaneously, the magnetic precession caused by the ac Josephson effect provides feedback to the supercurrent [8]. This bidirectional coupling of the two subsystems can produce chaotic dynamics.

Using the full spectrum Lyapunov exponent (LE) method [41–43], we found that two of the LEs are always zero. While such behavior is usually associated with a very particular type of chaos [44,45], here it is due to the conservation of the magnetic moment magnitude. We also show that, due to symmetry in the system, the effective dimension of the state space is reduced to a value below four, making hyperchaos, i.e., with two or more positive LEs, impossible.

In order to get a more complete picture of the dynamics, we developed a composite method, inspired by recent works on isospike diagrams [39,46], for constructing two-dimensional bifurcation diagrams to display the periodicity of regular regions and islands of synchronization in the parameter space. We also make use of recurrence plots [47–49] to gain further insight into the chaotic properties of the magnetic and superconducting subsystems.

The paper is organized as follows. The model and methods are introduced in Sec. II, while the details about numerical integration schemes are given in the Appendix. Section III discusses the appearance of chaos with two zero LEs and the absence of hyperchaos in the simulation results. Correlation between the magnetic and superconducting dynamics and the properties of regular and chaotic regions are examined in the bifurcation diagrams and recurrence plots of Sec. IV. Finally, Sec. V concludes the paper.

II. MODEL AND METHODS

The dynamics of the SFS junction is characterized by the coupling of the superconducting phase difference φ and magnetization $\mathbf{M}$ of the ferromagnetic (F) layer, and it can be described by the system of equations obtained from the Landau-Lifshitz-Gilbert (LLG) equation, the equation for the biased current of the resistively and capacitively shunted junction (RCSJ) model, and the Josephson relation for the phase difference and voltage. Magnetization dynamics is described by the LLG equation:

$$\frac{d\mathbf{M}}{dt} = -\gamma \mathbf{M} \times H_{\text{eff}} + \frac{\alpha}{M_0}\left(\mathbf{M} \times \frac{d\mathbf{M}}{dt}\right), \tag{1}$$

where γ is the gyromagnetic ratio, α is Gilbert damping, and $M_0 = |\mathbf{M}|$. The first term on the right-hand side of the equation describes the precession of magnetic moment $\mathbf{M}$ around the effective magnetic field H_{eff} given as

$$H_{\text{eff}} = \frac{K}{M_0}\left[Gr \sin\left(\varphi - r\frac{M_y}{M_0}\right)\hat{y} + \frac{M_z}{M_0}\hat{z}\right], \tag{2}$$

where K is the anisotropic constant. The parameter $G = E_J/(K\mathcal{V})$ represents the ratio between the Josephson energy and the magnetic anisotropy energy, where $E_J = \Phi_0 I_c/(2\pi)$ is the Josephson energy, Φ_0 is the flux quantum, I_c is the critical current, $\mathcal{V}$ is the volume of the F layer, $r = \nu_{\text{so}}/\nu_F$ is the Rashba-type parameter that characterizes the relative strength of the spin-orbit coupling, $l = 4h_{\text{ex}}L/\hbar\nu_F$, L is the length of the F layer, and h_{ex} is the exchange field of the F layer. The second term inside the sine function represents the phase shift $\varphi_0 = rM_y/M_0$. It is also assumed that the gradient of the spin-orbit potential is along the easy axis, which is taken to be along z.

In the underdamped case, the bias current I flows through the system according to the extended RCSJ model, which takes into account time derivatives of phase shift φ_0 given by the following equation:

$$I = \frac{\hbar C}{2e}\frac{d^2\varphi}{dt^2} + \frac{h_{\text{ex}}}{2eR}\left[\frac{d\varphi}{dt} - \frac{r}{M_0}\frac{dM_y}{dt}\right] + I_c \sin\left(\varphi - r\frac{M_y}{M_0}\right). \tag{3}$$

Here, C and R are the capacitance and resistance of the Josephson junction, respectively.

The Josephson relation for the phase difference and voltage is given by

$$V(t) = \frac{\hbar}{2e}\frac{d\varphi}{dt}. \tag{4}$$

Using the normalized variables $m_i = M_i/M_0$ ($i \equiv x, y, z$), and introducing $A = \omega_F/(1+\alpha^2)$ and $B = Gr$ for convenience,

the system of equations describing the φ_0 JJ becomes

$$\begin{aligned}
\dot{m}_x &= A\{-m_y m_z + B m_z \sin(\varphi - r m_y) \\
&\quad - \alpha[m_x m_z^2 + B m_x m_y \sin(\varphi - r m_y)]\}, \\
\dot{m}_y &= A\{m_x m_z - \alpha[m_y m_z^2 - B(m_z^2 + m_x^2)\sin(\varphi - r m_y)]\}, \\
\dot{m}_z &= A\{-B m_x \sin(\varphi - r m_y) - \alpha[B m_y m_z \sin(\varphi - r m_y) \\
&\quad - m_z(m_x^2 + m_y^2)]\}, \\
\dot{\varphi} &= V(t), \\
\dot{V} &= [I - V(t) + r\dot{m}_y - \sin(\varphi - r m_y)]/\beta_c, \qquad (5)
\end{aligned}$$

where $\beta_c = 2eI_cCR^2$ is the McCumber parameter and the overdot denotes the total derivative with respect to time. To afford the use of the same timescale in the LLG and RCSJ equations, the time is normalized to ω_c^{-1}, while ferromagnetic resonance frequency $\Omega_F = K\gamma/M_0$ is normalized to ω_c, i.e., $\omega_F = \Omega_F/\omega_c$, where $\omega_c = 2eI_cR/\hbar$ is a characteristic frequency of the junction. In these units the Josephson frequency $\omega_J = V$, where V denotes the time average of the instantaneous voltage, $V(t)$. The bias current I is normalized to the critical current I_c, and the voltage to $V_c = I_cR$.

The bidirectional nature of the coupling between the magnetic and superconducting subsystems can be seen clearly in Eq. (5). In one direction, the magnetic system influences the total current passing through the junction via the spin-orbit ($r\dot{m}_y$) and superconducting [$\sin(\varphi - r m_y)$] contributions appearing in the last two equations, which are for the junction. In the other direction, the phase oscillations of the junction influence the magnetic system via the terms proportional to B in the first three equations, which are for the magnetization components. Therefore, in contrast to previous studies, such as the chaos reported in Refs. [36–39], here the appearance of chaotic dynamics does not require an external (unidirectionally coupled) ac drive. The Josephson junction, which is itself being driven externally by the dc-bias current I and internally by the magnetic system, fulfills the role of an internal drive for the magnetic system. Furthermore, since the oscillations of the driven junction depart from being harmonic as the superconducting current becomes appreciable, one may expect that the driving provided by the junction can lead to more complicated dynamics in comparison to a magnetic system that is driven harmonically, as in Refs. [36–39].

To investigate the chaotic behavior of the system we will simulate the CVC, the maximal value of the magnetic component, the superconducting current, and the LE in a wide range of Josephson to magnetic energy ratios $G \in [0, 30]$. In accordance with experimental requirements, the ratio G can vary from $G \ll 1$ for materials with large anisotropy to $G \gtrapprox 100$ for smaller anisotropy [8]. The Gilbert damping is fixed to the value $\alpha = 0.01$.

In studies of chaos, it is of utmost importance to obtain highly accurate solutions to the systems of coupled differential equations that are being studied. For the problem at hand, we have compared different numerical solution schemes and shown how the use of a symplectic or pseudosymplectic scheme can eliminate certain numerical artifacts produced by non-symplectic methods (see, the Appendix).

III. CHAOS, BUT NO HYPERCHAOS, WITH TWO ZERO LYAPUNOV EXPONENTS

We will first concentrate on the appearance of chaos in the ferromagnetic resonance (FMR) region of the φ_0 Josephson junction. In this region a resonance occurs when the Josephson frequency becomes close to that of the FMR, i.e., when $\omega_J \approx \omega_F$. In contrast to ω_J, which changes according to the Josephson relation [the fourth relation in Eq. (5)], ω_F is the frequency of ferromagnetic resonance and is determined by the anisotropy constant. The parameters of the model G, r, and α affect the ferromagnetic resonance, which results in a damped nonlinear resonance [50]. Since there is no external driving, the resonance is innate to the system. In our simulations it manifests itself through the dependence of $\hat{m}_y$ (the maximal value of m_y) on the bias current, producing a peak centered on $\omega_J = \omega_F$. In the CVC, it appears as a resonance branch over a voltage interval that characterizes the width of the resonance. Subharmonics of the FMR frequency may also be observed in the $\hat{m}_y(I)$ dependence and CVC. Figure 1 shows the bias current dependence of the LEs, λ_i, CVC, and $\hat{m}_y$ at several different values of G. When the Josephson energy is much smaller than the magnetic anisotropy energy, i.e., for small values of G such as in Fig. 1(a) ($G = 0.15$), there is no chaos, as reflected by the negative maximal LE. The main peak resulting from the FMR (seen at $I \approx 0.48$) and two of its subharmonics (at $I \approx 0.29$ and 0.25) are clearly visible on the curve for $\hat{m}_y(I)$. For the larger value of $G = 1.01$ shown in Fig. 1(b), the amplitude of the m_y precession is generally larger than in (a), and the first signs of chaos appear near $I = 0.28$, where the maximal LE becomes positive and $\hat{m}_y$ reaches its maximal value. The chaos first appears in the subharmonic region, near the transition from the resistive to the superconducting state. With the further increase in G, as shown in Figs. 1(c) and 1(d), the chaos spreads to higher values of I, for distinct regions. In Fig. 1(d), for example, we can distinguish four chaotic regions. Another signature of chaos can be also seen in the behavior of $\hat{m}_y$, which reaches its maximal value whenever the maximal LE becomes positive.

It is well known that chaotic systems with dimensions larger than three can have either one or more positive LEs, one trivially zero exponent, and the rest all negative. If there is more than one positive exponent, the system is said to be hyperchaotic. For continuous time-dependent dynamical systems without a fixed point, there must always be at least one zero LE (called the trivial exponent) corresponding to the slowly changing magnitude of a principal axis tangent to the flow [43]. This general property of the LEs was originally observed by Benettin *et al.* [51] and later proved by Haken [52]. However, a close examination of the LE spectra obtained from all our simulations shows that, not only do we *never* see hyperchaos in this system, but we *always* have two trivially zero LEs. The reason for the two trivially zero exponents in our system can be traced back to the presence of the ferromagnetic weak link, which brings effectively only two extra degrees of freedom to the system, due to the conservation of magnetic moment ($|\mathbf{m}| = 1$). Thus, the second trivially zero exponent is due to perturbation (frame) vectors that align with the direction of the magnetization vector during the averaging process. On average, the growth of such vectors is zero due to the con-

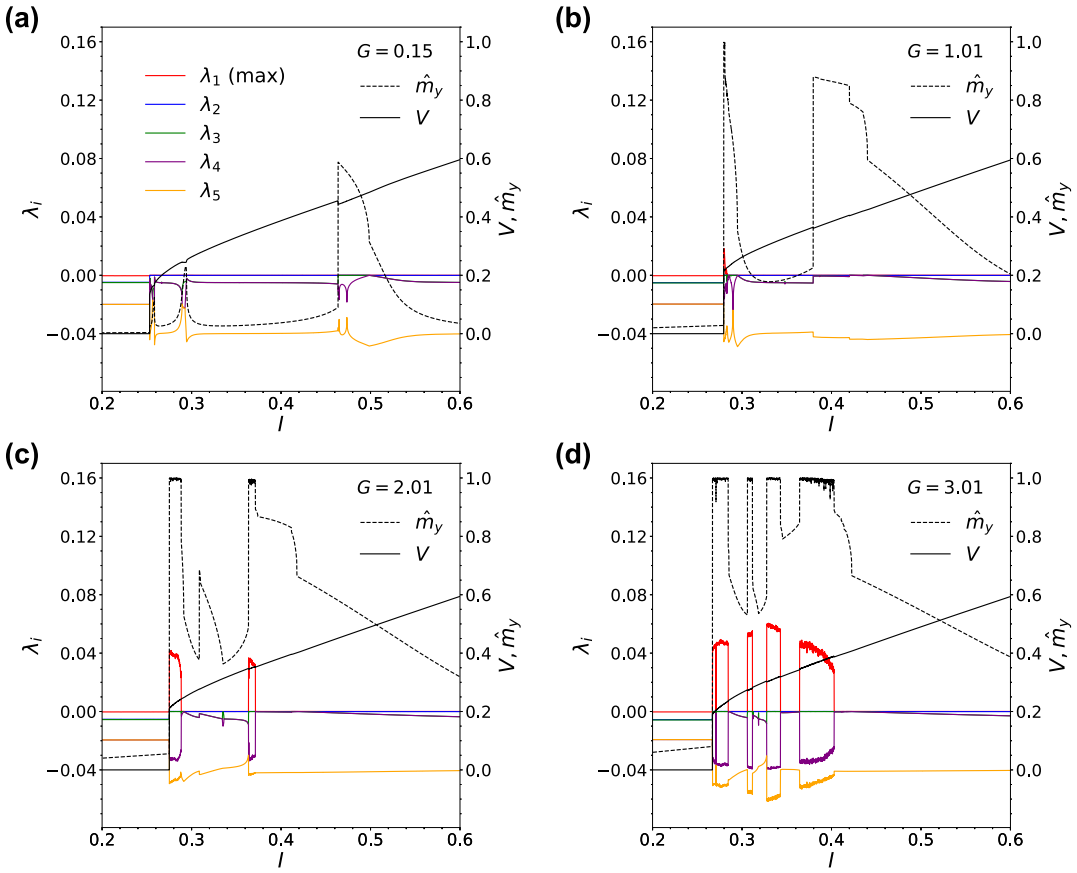

FIG. 1. Lyapunov exponents, λ_i, average voltage, V, and the maximum value of m_y, $\hat{m}_y$, as functions of the dc-bias current I. As shown by the legend in (a), the Lyapunov exponents have been ordered from largest to smallest, with the color codes λ_1 (red), λ_2 (blue), λ_3 (green), λ_4 (purple), and λ_5 (orange). (a) $G = 0.15$, (b) $G = 1.01$, (c) $G = 2.01$, and (d) $G = 3.01$. Other parameters: $\alpha = 0.01$, $r = 0.1$, $\beta_c = 25$, and $\omega_F = 0.5$.

servation of $|\mathbf{m}|$. On the other hand, the absence of hyperchaos is related to an inherent symmetry in the system: it is easy to see that the transformation $(m_x, m_y, m_z) \to (-m_x, m_y, -m_z)$ does not change the form of Eqs. (5). This means that, for every solution $(m_{x0}, m_{y0}, m_{z0}, \varphi_0, V_0)$ there is a mirror reflected solution $(-m_{x0}, m_{y0}, -m_{z0}, \varphi_0, V_0)$ [6]. Now, as we have observed, the system is chaotic only when the oscillations in m_y reach their maximal amplitude ($m_y = 1$). At $m_y = 1$ the other two components of magnetization are necessarily zero, and at such a point the system may thus follow either the $m_x, m_z > 0$ or $m_x, m_z < 0$ solution, with equal probability. On the other hand, as long as $\hat{m}_y < 1$, there is no possibility for the solution to jump between the two mirror image solutions. Recently, a similar symmetry relation was identified in connection with intermittent chaos in the driven LLG equation [53]. It was found that, during the "relaminarization phases" at the end of each turbulent burst, the system returns (randomly) to either of the two symmetry-related limit cycles. Similarly, in our system, we see that a chaotic solution may jump intermittently between two symmetry-related chaotic attractors. The coexistence of these attractors effectively reduces the available state space for each attractor separately, thus precluding the possibility of hyperchaos.

As we saw in Fig. 1, the behavior of the system becomes increasingly complicated with increasing G. For values of G higher than those shown in Fig. 1, the behavior can consist of multiple transitions between periodic, quasiperiodic, and chaotic areas, as the bias current is varied. To illustrate this more clearly, we have also simulated bifurcation diagrams at much higher values of G, as shown in Fig. 2, for decreasing I. In Fig. 2(a), we see period two behavior down to about $I = 0.515$, and thereafter period one until the quasiperiodic (QP) region between $I = 0.461$ and $I = 0.443$. Immediately to the left of the QP region, the system is again periodic (period five), before transitioning through a series of period-doubling bifurcations and becoming chaotic at $I = 0.426$. As I decreases further, the system is chaotic, interrupted by small periodic windows, down to $I = 0.26$ where the junction reenters the superconducting state. As G increases, i.e., as the Josephson energy becomes larger in comparison to the magnetic energy, as in Figs. 2(b) and 2(c), the chaotic region shrinks, and the QP region moves to a higher current. The QP region can be recognized in Fig. 2(b) at around $I = 0.61$, whereas in Fig. 2(c) it has shifted further up, off the scale. In Fig. 2(b) we see also a narrow chaotic region appearing around $I \approx 0.56$.

The Lyapunov exponents and $\hat{m}_y$, both as functions of decreasing I at $G = 5.01$ and $\alpha = 0.01$, are shown in Fig. 3(a). In Figs. 3(b) and 3(c) the corresponding CVC is plotted together with the bifurcation diagrams for m_y and m_z. Again as

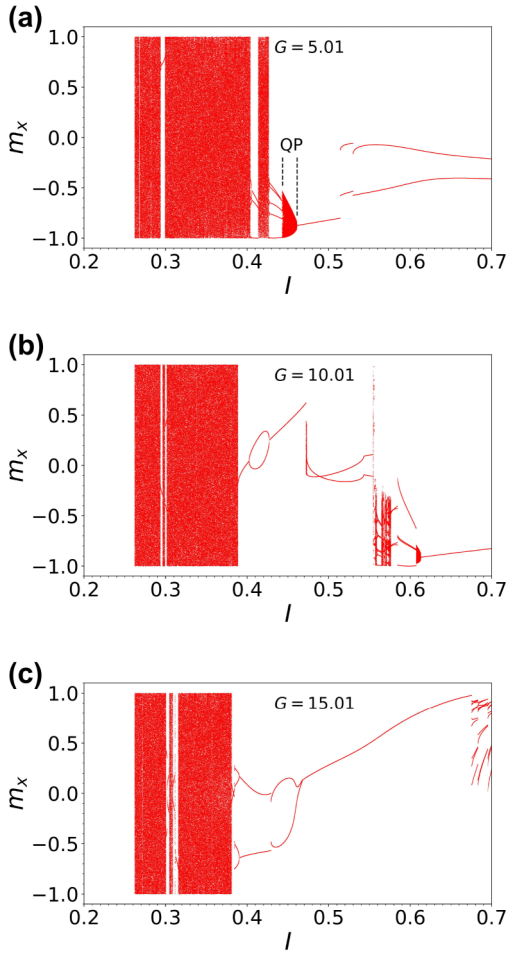

FIG. 2. Bifurcation diagrams for m_x, plotted when $\sin(\phi - rm_y)$ crosses from negative to positive. (a) $G = 5.01$, (b) $G = 10.01$, and (c) $G = 15.01$. The vertical dashed lines in (a) show a QP region, as described in the main text. Other parameters as in Fig. 1.

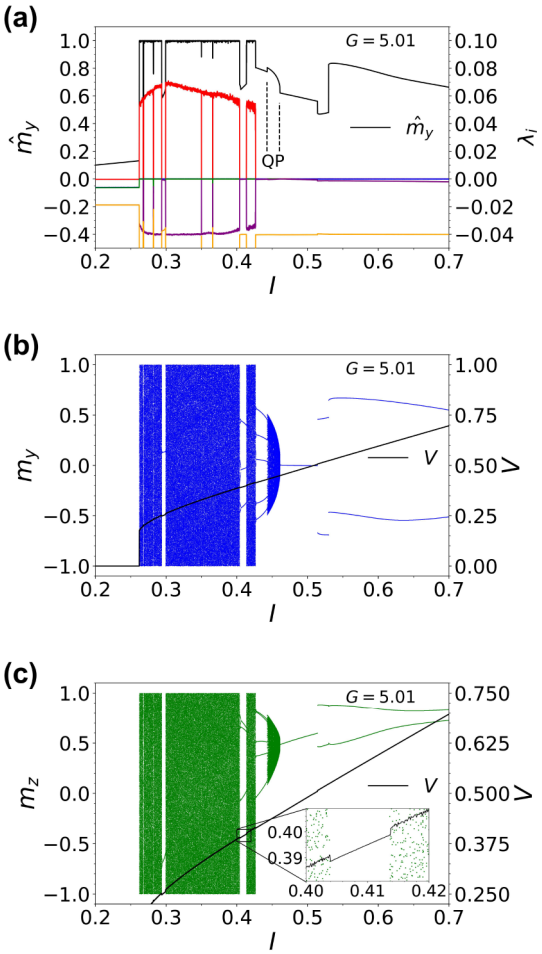

FIG. 3. Seen as functions of decreasing dc-bias current, I, and for $G = 5.01$, (a) Lyapunov exponents and maximal value of m_y, denoted by $\hat{m}_y$. For the bias current interval shown between the vertical dashed lines, $I \in (0.4426, 0.4602)$, two maximal exponents are simultaneously equal to zero, indicating two-frequency QP behavior. (b),(c) Bifurcation diagrams for m_y and m_z, respectively, are both plotted when $\sin(\phi - rm_y)$ crosses from negative to positive, together with the CVC (black solid line). The inset in (c) shows a magnified view of the CVC, where there is a sudden voltage decrease as the dynamics changes from chaotic to periodic. Within the periodic window seen here, we have period 3 behavior, bifurcating to period 6, before becoming chaotic as the current decreases. Other parameters as in Fig. 1.

in Fig. 1, the magnetization only attains the value $|\hat{m}_y| = 1$, when the system is chaotic. Periodic windows within chaotic regions exhibit period-doubling bifurcations leading to chaos. Within the window surrounding $I = 0.41$, for example, we see period 3 behavior, bifurcating to period 6, before becoming chaotic. A magnified view of the CVC within the window is shown in the inset of Fig. 3(c), clearly showing a sudden voltage decrease as the dynamics changes from chaotic to periodic within the window.

IV. CHAOS-I_S CORRELATIONS AND FREQUENCY SYNCHRONIZATION

In this section, we will further examine the correlation between the behavior of magnetic moment and the superconducting current, their periodicity, and the synchronization between the magnetic and superconducting variables. In Fig. 4, the phase diagrams for the maximal LE and the superconducting current I_s as functions of the dc-bias current I and the parameter G (the ratio between the Josephson energy and the magnetic anisotropy energy) are presented in Figs. 4(a) and 4(b), respectively. This figure was generated starting from the initial condition $(1/\sqrt{3}, 1/\sqrt{3}, 1/\sqrt{3}, 0, 0)$ at $I = 1.1$, and slowly sweeping the dc-bias current downwards in steps of $\Delta I = -0.0001$. Here we have allowed a transient time of 256 000 between each I, before averaging the exponents over an additional 128 000 time units. For any given value of G where $G \leqslant 1$, there is a threshold value of the bias current after which chaos starts to appear. As we can see the chaotic regions have a "tree"-like shape where the chaotic areas are alternating with regular regions. Small I makes the appearance of chaos very difficult, but the increase in G leads to the appearance of chaos at a smaller current, thus we see the left edge of the chaotic region tilting slightly towards the lower I as G increases. The correlation between the behavior of the magnetic moment and the superconducting current can be seen in Fig. 4(b) where I_s exhibits the very same treelike

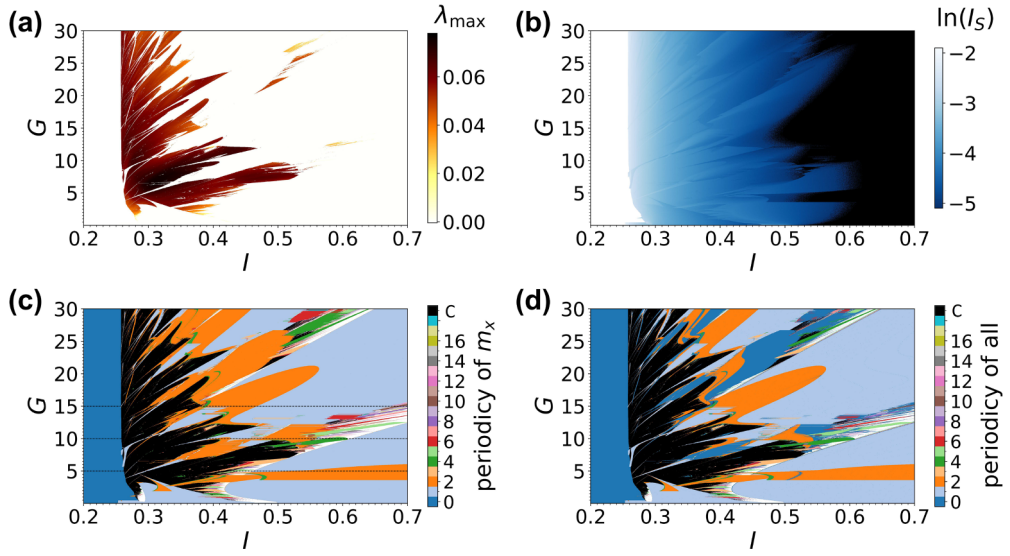

FIG. 4. (a) Maximal Lyapunov exponent as a function of G (the ratio between the Josephson energy and the magnetic anisotropy energy), and the dc-bias current, I. (b) The superconducting current I_s as a function of I and G. (c) Two-dimensional bifurcation diagrams for m_x, plotted when $\sin(\phi - rm_y)$ crosses from negative to positive. The periodicity has been indicated by the color scale, from zero (no oscillations) to period 18. The black color, labeled as C, indicates the chaotic regions, while any quasiperiodic regions have been colored white (not shown on the color scale). The three horizontal lines are there to guide the eye for the values $G = 5.01$, 10.01, and 15.01 discussed previously in Fig. 2. (d) Regions of synchronization where all five state variables (m_x, m_y, m_z, ϕ, and V) have the same periodicity indicated by the same color scale as in (c). Here, the regular regions, where variables are not synchronized, are marked by the color 0. In all four figures the fixed parameters are the same as in Fig. 1.

structure as the LE in Fig. 4(a), which is a direct consequence of bidirectional coupling.

The LE phase diagram clearly reveals chaotic regions in parameter space; however, the properties of regular ones, except that they are not chaotic, remain completely unknown. To gain insight into the regular areas in Fig. 4(a) we introduce a particular type of two-dimensional bifurcation diagram (2DBD), which, in addition to chaotic regions, reveals a complex network of different periodic domains and synchronized regions. In Fig. 4(c), 2DBD for m_x, plotted when $\sin(\phi - rm_y)$ crosses from negative to positive, is presented. The periodicity of regular regions is indicated by the color scale starting from zero (no oscillations), period 1 in light blue, period two in orange, etc., while the chaotic and quasiperiodic areas are indicated by the black and white regions, respectively. The three horizontal lines are there to guide the eye to the values G which correspond to the bifurcation diagrams in Fig. 2. In addition to the chaotic regions, in Fig. 4(a), the 2DBD in Fig. 4(c) reveals a very complex treelike structure consisting of chaotic areas alternating with regular areas of different periodicity. The chaotic areas are usually surrounded by regions of periodicity two (orange). At a certain value of G we can see the first two period-doubling bifurcations leading to chaos, i.e., part of the sequence: orange, green,..., black. This is seen, for example, by comparing Fig. 2(c) with 4(c) at $G = 15$ and $I \approx 0.4$. Unlike chaos, which is found in the ferromagnetic resonance region, the quasiperiodic behavior (white areas) of magnetization usually appears far from the resonance. Here we presented only the results for m_x, but similar plots were also made for other variables.

Since we have five state variables (m_x, m_y, m_z, ϕ, and V), the question that arises is whether there are regular areas where all of them have the same periodicity, i.e., where they are all synchronized. In Fig. 4(d), using a color scale, we presented areas of synchronicity where all five state variables (m_x, m_y, m_z, ϕ, and V) have the same periodicity (each periodicity is marked by a different color). The blue color, corresponding to zero, corresponds to regular regions in which there is no frequency synchronization. We see that if all five variables are synchronized, their periodicity is either one or two, and it is very difficult for them to synchronize at a larger periodicity. Much smaller areas in which there is frequency synchronization at larger periodicities (periods 4, 6, and higher), do appear in the region $I \in (5.5, 6.5)$ and $G \approx 10$. This plot reveals a very complex picture of different chaotic scenarios: in some cases, the chaotic areas are separated by perfectly synchronized regions usually of periodicity 1 or 2, but sometimes those regions become quasiperiodic and desynchronized before becoming chaotic.

In two recent papers on the dynamics of the SFS φ_0 Josephson junction [50,54], it was shown that in the resonance regime, $\omega_J \approx \omega_F$, for a certain range of the parameters G, α, and r, the system of equations can be reduced to a Duffing equation for the m_y dynamics, driven by the Josephson current as the external stimulus of frequency ω_J. In the Duffing oscillator the interplay between internal and forcing frequency can lead to periodic or quasiperiodic transients with rational or irrational ratios of frequencies, respectively. Such transient regions are referred to as Arnold tongues [55]. In general, for certain system parameters, the Arnold tongues start to overlap and the system becomes chaotic [56]. The so-called intermingled Arnold tongues were observed in the Duffing system, not only in the case of low but also in the case of high dissipation [55]. The number of degrees of freedom allows

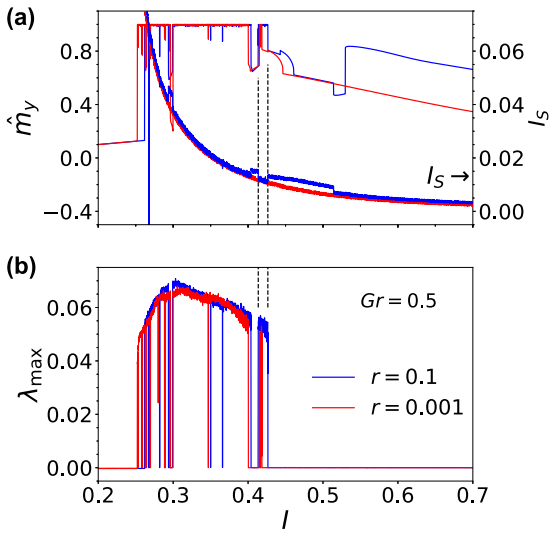

FIG. 5. (a) $\hat{m}_y$ (left axis), and superconducting current, I_s (right axis), as a function of decreasing bias current, for two different values of spin-orbit coupling: $r = 0.1$ in blue and 0.001 in red. In both cases, G is adjusted so that drive amplitude $Gr = 0.5$, is the same. (b) The maximal Lyapunov exponents corresponding to the two cases in (a). The vertical dashed lines are there to guide the eye. In the chaotic regions, indicated by $\lambda_{\max} > 0$, $\hat{m}_y \approx 1$, and I_S for both cases practically coincide. See main text for details.

for chaos in the dynamics of the precessing magnetic moment with Gilbert damping. The reduction to a single Duffing oscillator holds only for small parameters. For large parameters, the Duffing system still develops chaos, with the so-called intermingled Arnold tongues [55]. Here, we have shown that, for large parameters, the model of the SFS φ_0 junction develops chaos through complex interwoven dynamics of the magnetic moment and the Josephson current, each affecting the other, simultaneously. Our results in Figs. 4(c) and 4(d) show that a pattern similar to the intermingled set of period-q tongues develops also in our model, bringing about a particular correlation among the resonances of various orders, as the supercurrent takes on larger values. Similar to the Duffing oscillator [55], the chaotic attractor for our bidirectional model develops for higher dissipation.

To understand the effect of the bidirectional coupling, we perform analysis also for the case when r is near zero. In Fig. 5(a), $\hat{m}_y$ (left axis), and superconducting current, I_s (right axis), as a function of decreasing bias current for two different values of spin-orbit coupling: $r = 0.1$ in blue and 0.001 in red are presented. In both cases, G is chosen so that drive amplitude, $B = Gr = 0.5$, is the same. As we can see from the last equation in Eqs. (5), for $r \approx 0$, m_y will have almost no effect on the junction. However, since $B = 0.5$, the junction still drives the magnetic system in approximately the same way as in the model of the LLG equation with a constant longitudinal and harmonic transverse external magnetic field [37,38]. In Fig. 5(a) for $r \approx 0$ (in red), we see that I_s is unaffected by m_y, which is not the case for $r = 0.1$ (in blue). However, when the frequency of the junction changes as the dc-bias current is swept down, the junction behaves increasingly anharmonically, as evidenced by the rising I_s. For higher I, i.e., when $I_s \approx 0$, the junction becomes essentially harmonic, while only at the bias current close to the transition to the superconducting state, does the junction show any appreciable anharmonicity. It is only when the system becomes chaotic that the I_s (blue and red) curves coincide, as can be seen, if we look between the two vertical dashed lines. This indicates that in the chaotic state, the magnetic system in fact has very little effect on the junction, irrespective of the value of r. On the other hand, as Fig. 5(b) shows, the chaotic behavior appears in both cases because the magnetic moment is being driven by the superconducting current.

It is interesting to note that the results in Fig. 5, as well as those in Figs. 1–3, indicate that the maximum value of magnetization components only reaches 1 when the system is chaotic. To gain insight into this behavior, we have constructed recurrence plots from the time series of the dynamical variables in the chaotic region. A recurrence plot (RP) is an advanced technique for nonlinear data analysis, used to visualize how often and how close the trajectory of the dynamical system revisits areas in the phase space [48]. In its simplest form, it is a visualization of a square matrix, in which the column and row indices correspond to a certain pair of equally spaced sample times from the system trajectory. The value of any particular element in the matrix represents the spatial distance between two samples. In this way, distance correlations in a time series can be identified. In the case of only the magnetic coordinates, for example, the recurrence matrix elements are

$$R_{i,j} = \sqrt{\sum_{\ell=\{x,y,z\}} [m_\ell(t_i) - m_\ell(t_j)]^2}, \tag{6}$$

where t_i is the time at which the trajectory is sampled.

In Fig. 6, the RPs for the magnetic system coordinates, junction coordinates, and all five coordinates are presented in (a)–(c), respectively. The RPs for only the magnetic coordinates (a), and all five coordinates (c), are typical for chaotic dynamics involving a repeating phase. We see that the blue color corresponding to close recurrences forms short—irregular in length—diagonal striations that are mostly parallel to the line of identity. This pattern is comparable to the *periodic* typology described in Fig. 4 of Ref. [47] and is consistent with there being some inherent oscillations (not exactly periodic) superimposed on the chaotic motion. In (a), we also observe that the maximum separation of the sampled points is 2, in agreement with Figs. 2 and 3, where we observed that, in the chaotic regions of the bifurcation diagrams, the components of the magnetization traversed the full available range, $[-1, +1]$. In (a), the red regions thus correspond to recurrences of the maximal separation on the surface of the unit sphere $|\mathbf{m}|$. The exquisite structure seen in the way the magnetization revisits points on the sphere is due to the deterministic nature of the chaos seen here, as opposed to stochastic chaos. The more regular structure seen in Fig. 6(b) for the junction coordinated due to the repeating phase of the junction rotations. Inherently, the junction can only be chaotic by rotating at variable angular speed. Here its speed is modulated through the coupling to the magnetic moment making it "not quite periodic" [47].

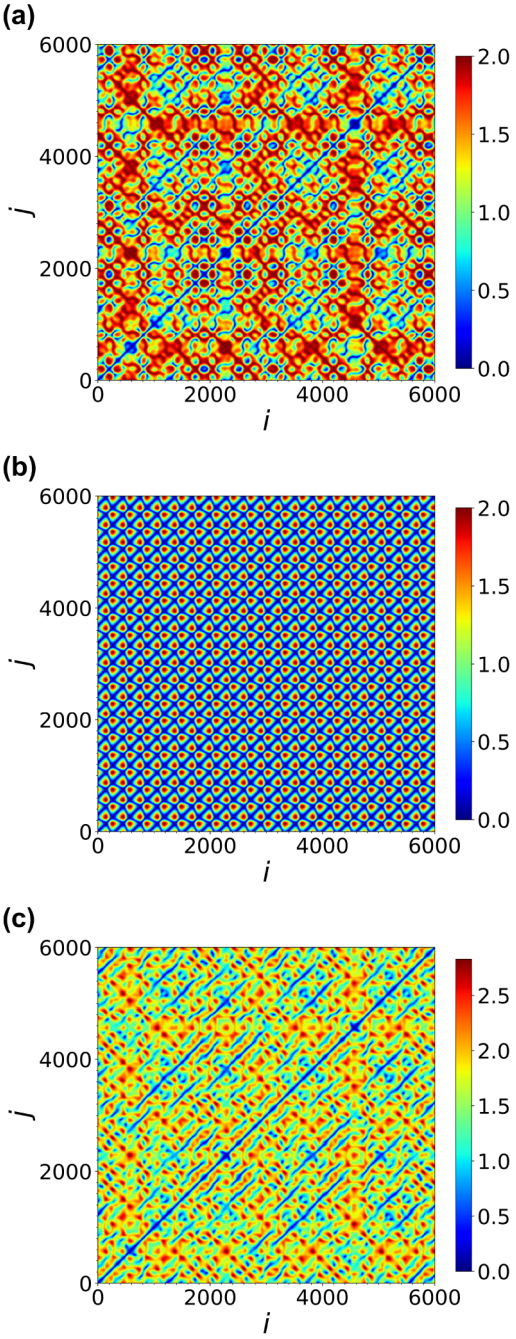

FIG. 6. Recurrence plots for (a) the magnetic system coordinates (m_x, m_y, m_z), (b) the junction coordinates $(\sin\varphi, V)$, and (c) all five coordinates $(m_x, m_y, m_z, \sin\varphi, V)$. We used $\sin\varphi$ instead of φ to avoid problems with the unbounded phase. The color scale indicates the distance between the coordinates at times corresponding to $i, j = 0, 1, \ldots, 6000$. A chaotic time series of length 375 was sampled at intervals of $\Delta t = 1/16$, to produce the sequence of 6000 data points. $I = 0.35$, with the remaining parameters as in Fig. 2(b).

V. CONCLUSION

In this work, it was demonstrated that the SFS φ_0 Josephson junction could become chaotic without any external drive, due to the presence of the ferromagnetic weak link, in which the precessing magnetic moment, $|\mathbf{m}|$, was bidirectionally coupled to the supercurrent through the junction. We emphasized that, in numerical studies of this system, it was important to use an integration method that conserves $|\mathbf{m}|$ to high accuracy, since exceedingly long transient times could occur. In the Appendix, we evaluated the performance of different integration schemes and concluded that an explicit pseudosymplectic method can provide much faster results while being almost as accurate as an implicit method that strictly conserved $|\mathbf{m}|$. We found that two, as opposed to the usual one, of the five Lyapunov exponents were trivially zero due to the conservation of $|\mathbf{m}|$, and symmetry in the dynamical equations precluded the occurrence of hyperchaos (with two positive maximal Lyapunov exponents), due to the reduction of the effective state space dimension to below four. The correlation between the behavior of magnetic moment and supercurrent was demonstrated through two-dimensional bifurcation diagrams which displayed a very complex landscape of quasiperiodic, chaotic, and regular regions; the latter, showing a variety of different periodicities and synchronization regions. Recurrence plots were also presented as a visualization of these complex dynamics, in an attempt to understand the correlation between the occurrence of chaos (positive maximal LE) and the magnetization components reaching their maximal values of ± 1.

The present studies were mainly focused on the influence of the Josephson to magnetic energy ratio, while the effects of varying other parameters such as Gilbert damping or spin-orbit coupling were not explored in detail. Thus, expanding the present study to consider also the influence of the other parameters could broaden our present understanding of chaos in the SFS φ_0 junction. For example, it could be interesting, though computationally very expensive, to make higher resolution plots of the shrimplike periodic islands and other structures we observed within the chaotic regions, as was done in Refs. [36,39], for an ac-driven magnetic monodomain model of a nanoparticle.

Recently, it was suggested that the introduction of an ac drive of specific amplitude and frequency could suppress chaos in a related system [57]. The drive expanded the effective state space dimension to greater than four, thereby making hyperchaotic behavior possible, though yet to be confirmed. We anticipate that, with ac driving, a similar scenario may occur in the present system. The transition in going from chaos in the autonomous system to the potentially hyperchaotic response in the ac-driven system could also be an interesting future study, particularly from the viewpoint of developing chaos control strategies for the SFS φ_0 junction.

As another extension of the present work, one or more metrics could be used to perform recurrence quantification analysis [49] on several different chaotic time series sampled over a wider range of currents. Such a study could provide further insights into the dynamics of the underlying chaotic attractor.

ACKNOWLEDGMENTS

A.E.B. acknowledges use of the high-performance computing facility at the University of South Africa. Yu.M.S. would like to acknowledge the financial support by the Russian Science Foundation, Project No. 22-71-10022. J.T. would like to acknowledge the financial support by the Ministry of

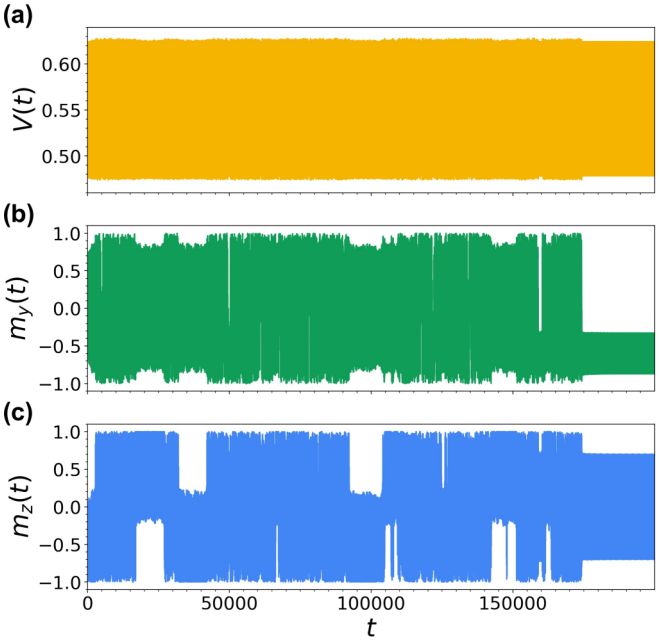

FIG. 7. Time series for (a) $V(t)$, (b) $m_y(t)$, and (c) $m_z(t)$, at a dc-bias current of $I = 0.554\,06$. We see that transient chaos persists in this case until $t \approx 175\,000$, after which the system relaxes into stable periodic behavior. To generate these results we have employed a second-order implicit Gauss-Legendre integration scheme that conserves $|\mathbf{m}|$ to within the numerical tolerance of the root finding algorithm (in this case $\lessapprox 10^{-14}$). To solve the implicit equation we use the Newton-Raphson method without making any approximations to calculate the inverse of the Jacobian matrix [58]. We use a fixed time step, $\Delta t = 0.01$. Other parameters are $\alpha = 0.01$, $r = 0.1$, $G = 10$, $\omega_F = 0.5$, and $\beta_c = 25$.

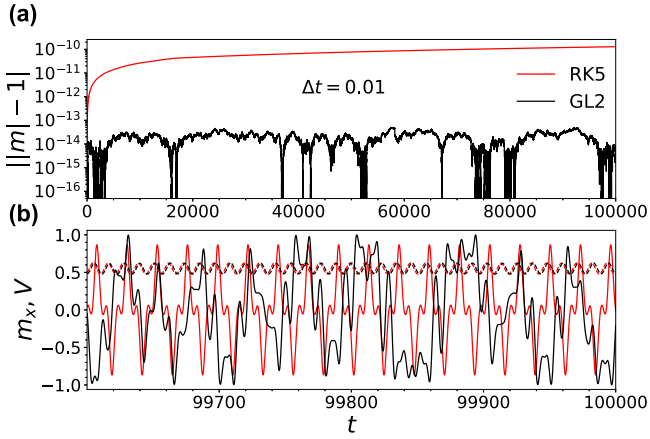

FIG. 8. Comparison of the fifth-order explicit Runge-Kutta method (RK5), with the implicit second-order Gauss-Legendre method (GL2) for $I = 0.554\,00$. All other parameters and the initial conditions are the same as in Fig. 7, for both methods employed here. (a) The absolute value of the error $|\mathbf{m}| - 1$, plotted on a logarithmic scale, showing the extent to which each method conserves $|\mathbf{m}|$. (b) Last part of the time series for m_x and V, for each method. Notably, the time series from the RK5 method is regular, while that from the GL2 method is chaotic, highlighting the importance of choosing the correct integration scheme in numerical studies of this system.

Education, Science and Technological Development of the Republic of Serbia, Grant No. 451-03-68/2022-14/200017 ("Vinča" Institute of Nuclear Sciences, University of Belgrade). M.R.K. would like to acknowledge the support of the Institute for Advanced Studies in Basic Sciences (IASBS).

APPENDIX: COMPARISON OF DIFFERENT INTEGRATION SCHEMES

To simulate the present system as accurately as possible, it is important to select a numerical integration scheme that conserves the magnitude of the magnetization, $|\mathbf{m}|$, over the relatively long simulation times required to compute averaged quantities, such as the Lyapunov exponents and CVC. This is especially important since the magnetic system is lightly damped for $\alpha = 0.01$, giving rise to transient times that can be on the order of 10^5 dimensionless time units. While in reality such transients are not physically significant—in real time they are extremely short-lived—in comparison to the accessible timescales that can be simulated numerically, they can span a large fraction of the total simulation time. Thus, long simulation times are required to eliminate transients in the system, before time averaging.

As an extreme example of such transient behavior, Fig. 7 shows the time series of the voltage and two of the magnetization components when Eq. (5) is solved at $I = 0.554\,06$. As mentioned in the main text, to eliminate such transients, we have first integrated over 256 000 dimensionless time units, before averaging.

In the present work, we have used a second-order implicit Gauss-Legendre method (GL2) to perform the integration in a manner that ensures that $||\mathbf{m}| - 1| \lessapprox 10^{-14}$ over the total required integration time. Figure 8 shows a comparison between the GL2 method, used in Fig. 7, and an explicit fifth-order Runge-Kutta method (RK5). Here the bias current $I = 0.554\,00$ is only slightly different from that used in Fig. 7, with all the other parameters and initial conditions being the same. Despite the higher order of the explicit RK5 method, we see in Fig. 8(a), that the error in $||\mathbf{m}| - 1|$ grows linearly with time for the RK5 method, while the error associated with the GL2 method remains approximately below 10^{-14}, over the entire integration time. We have tested that linear growth in $||\mathbf{m}| - 1|$ also occurs for the standard and modified fourth-order Runge-Kutta integration schemes which have been used in Refs. [37] and [53], respectively, for studying chaos in magnetization dynamics.

In Fig. 8(b) one can visually see how the choice of the integration scheme can affect the nature of the solution. In this case, starting from precisely the same initial conditions, after 100 000 integration time units the last part of the trajectory from the RK5 method shows that the trajectory has settled into periodic behavior, whereas the last part of the trajectory from the GL2 method is clearly chaotic. Such differences highlight the importance of using an integration method that conserves the magnitude of the magnetization field to a high accuracy. The use of the pseudosymplectic (PS) numerical integration techniques for Landau-Lifshitz dynamics have recently been considered in Ref. [59]. We have therefore also compared

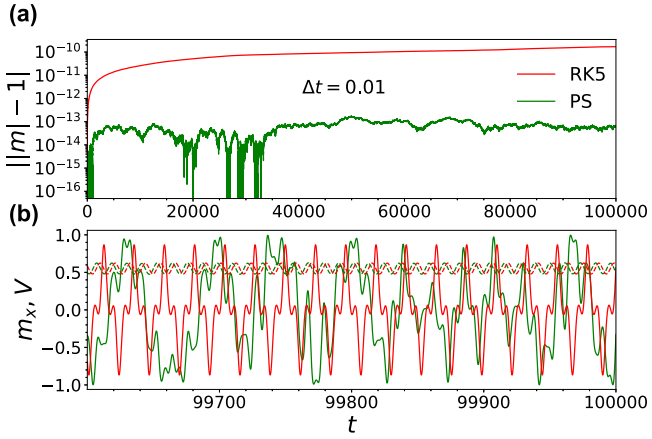

FIG. 9. Comparison of the fifth-order explicit Runge-Kutta method (RK5), with the pseudosymplectic (PS) method of the same order. All parameters and the initial conditions are the same for both methods, as in Fig. 8. (a) The absolute value of the error $|\mathbf{m}| - 1$, plotted on a logarithmic scale, showing the extent to which each method conserves $|\mathbf{m}|$. (b) Last part of the time series for m_x and V, for each method. Notably, the time series from the RK5 method is regular, while that from the PS method is chaotic, in qualitative agreement with the results from the GL2 method (cf. Fig. 8).

the explicit RK5 method to an explicit PS method, referred to as 4p7q(6) in Ref. [60], which is not only substantially faster than the GL2 method but also gives results that are in very close agreement with those from the GL2 method. In Fig. 9(a) we compare the errors from the explicit RK5 and PS methods. The error from RK5 is as before, while one can see that the error from the PS method is substantially lower, being almost comparable to that of the GL2 method (cf. Fig. 8). Importantly, both the GL2 and PS methods are in agreement insofar as they both produce a chaotic trajectory at the end of the integration period. After more extensive comparisons like those of Figs. 8 and 9, we concluded that the GL2 and PS methods produce chaotic transient times that are in close agreement, meaning that the PS method is sufficiently accurate for studying chaos in the present system. Since the PS method is almost an order of magnitude faster than GL2, it offers a substantial advantage when generating results that involve large amounts of CPU time, such as those of Fig. 4.

Finally, we note that, at the parameters of interest, we have not been able to detect any intermittent chaos in our system, i.e., once a transient chaotic trajectory settles into regular behavior, as shown in Figs. 8 and 9, for example, it does not become chaotic again, even for integration times up to 1×10^6 dimensionless time units. Of course, this does not prove that intermittent chaos is impossible in our system, but merely that it may be rare. Indeed, type-III intermittency has only recently been reported for the dissipative LLG equation representing the magnetization dynamics of an anisotropic nanoparticle subjected to a time-variant magnetic field [53].

[1] M. Eschrig, Spin-polarized supercurrents for spintronics, Phys. Today **64**(1), 43 (2011).

[2] V. V. Ryazanov, V. V. Bol'ginov, D. S. Sobanin, I. V. Vernik, S. K. Tolpygo, A. M. Kadin, and O. A. Mukhanov, Magnetic Josephson junction technology for digital and memory applications, Phys. Procedia **36**, 35 (2012).

[3] J. Linder and J. W. Robinson, Superconducting spintronics, Nat. Phys. **11**, 307 (2015).

[4] A. A. Golubov and M. Y. Kupriyanov, Controlling magnetism, Nat. Mater. **16**, 156 (2017).

[5] Yu. M. Shukrinov, Anomalous Josephson effect, Phys. Usp. **65**, 317 (2022).

[6] Yu. M. Shukrinov, I. R. Rahmonov, and A. E. Botha, Dynamics of anomalous Josephson effect in superconducting nanostructures, in *Low-Dimensional Materials: Theory, Modeling, Experiment, Dubna 2021*, edited by V. A. Osipov and V. L. Katkov, AIP Conf. Proc. No. 2551 (AIP, Melvile, NY, 2022), p. 020003.

[7] A. Buzdin, Direct Coupling between Magnetism and Superconducting Current in the Josephson φ_0 Junction, Phys. Rev. Lett. **101**, 107005 (2008).

[8] F. Konschelle and A. Buzdin, Magnetic Moment Manipulation by a Josephson Current, Phys. Rev. Lett. **102**, 017001 (2009).

[9] S. Takahashi, S. Hikino, M. Mori, J. Martinek, and S. Maekawa, Supercurrent Pumping in Josephson Junctions with a Half-Metallic Ferromagnet, Phys. Rev. Lett. **99**, 057003 (2007).

[10] D. Szombati, S. Nadj-Perge, D. Car, S. Plissard, E. Bakkers, and L. Kouwenhoven, Josephson φ_0-junction in nanowire quantum dots, Nat. Phys. **12**, 568 (2016).

[11] A. Assouline, C. Feuillet-Palma, N. Bergeal, T. Zhang, A. Mottaghizadeh, A. Zimmers, E. Lhuillier, M. Eddrie, P. Atkinson, M. Aprili *et al.*, Spin-orbit induced phase-shift in Bi_2 Se_3 Josephson junctions, Nat. Commun. **10**, 126 (2019).

[12] W. Mayer, M. C. Dartiailh, J. Yuan, K. S. Wickramasinghe, E. Rossi, and J. Shabani, Gate controlled anomalous phase shift in Al/InAs Josephson junctions, Nat. Commun. **11**, 212 (2020).

[13] V. Eclerová, L. Přibylová, and A. E. Botha, Embedding nonlinear systems with two or more harmonic phase terms near the Hopf-Hopf bifurcation, Nonlinear Dyn. **111**, 1537 (2023).

[14] R. L. Kautz and R. Monaco, Survey of chaos in the rf-biased Josephson junction, J. Appl. Phys. **57**, 875 (1985).

[15] K. K. Likharev, *Dynamics of Josephson Junctions and Circuits* (Gordon and Breach, New York, 1986).

[16] R. Kleiner and R. P. Huebener, *Superconductivity: Fundamentals and Applications* (Wiley-VCH, Berlin, 2004).

[17] M. Basler, W. Krech, and K. Y. Platov, Theory of phase locking in small Josephson-junction cells, Phys. Rev. B **52**, 7504 (1995).

[18] J. Hassel, L. Grönberg, P. Helistö, and H. Seppä, Self-synchronization in distributed Josephson junction arrays studied using harmonic analysis and power balance, Appl. Phys. Lett. **89**, 072503 (2006).

[19] R. Bhagavatula, C. Ebner, and C. Jayaprakash, Spatiotemporal chaos in Josephson-junction arrays, Phys. Rev. B **50**, 9376 (1994).

[20] A. A. Chernikov and G. Schmidt, Adiabatic chaos in Josephson-junction arrays, Phys. Rev. E **50**, 3436 (1994).

[21] Z. Tie-Ge, M. Jing, L. Ting-Shu, L. Yue, and Y. Shao-Lin, Phase locking and chaos in a Josephson junction array shunted by a common resistance, Chin. Phys. Lett. **26**, 077401 (2009).

[22] I. Ri, Y.-L. Feng, Z.-H. Yao, and J. Fan, Hyperchaotic behaviours and controlling hyperchaos in an array of RCL-shunted Josephson junctions, Chin. Phys. B **20**, 120504 (2011).

[23] Y.-L. Feng, X.-H. Zhang, Z.-G. Jiang, and K. Shen, Generalized synchronization of chaos in RCL-shunted Josephson junctions by unidirectionally coupling, Int. J. Mod. Phys. B **24**, 5675 (2010).

[24] C. B. Whan and C. J. Lobb, Complex dynamical behavior in RCL-shunted Josephson tunnel junctions, Phys. Rev. E **53**, 405 (1996).

[25] A. S. P. Komnang, C. Guarcello, C. Barone, C. Gatti, S. Pagano, V. Pierro, A. Rettaroli, and G. Filatrella, Analysis of Josephson junctions switching time distributions for the detection of single microwave photons, Chaos, Solitons Fractals **142**, 110496 (2021).

[26] Yu. M. Shukrinov, M. Hamdipour, M. R. Kolahchi, A. E. Botha, and M. Suzuki, Manifestation of resonance-related chaos in coupled Josephson junctions, Phys. Lett. A **376**, 3609 (2012).

[27] A. E. Botha, Yu. M. Shukrinov, and M. R. Kolahchi, Onset of chaos in intrinsic Josephson junctions, Chaos, Solitons Fractals **48**, 32 (2013).

[28] B. Huberman, J. Crutchfield, and N. Packard, Noise phenomena in Josephson junctions, Appl. Phys. Lett. **37**, 750 (1980).

[29] R. L. Kautz, Chaotic states of rf-biased Josephson junctions, J. Appl. Phys. **52**, 6241 (1981).

[30] R. L. Kautz, Chaos and thermal noise in the rf-biased Josephson junction, J. Appl. Phys. **58**, 424 (1985).

[31] A. Irie, Y. Kurosu, and G. Oya, RF-induced steps in intrinsic Josephson junctions in $Bi_2Sr_2CaCu_2O_y$, IEEE Trans. Appl. Supercond. **13**, 908 (2003).

[32] J. Scherbel, M. Mans, H. Schneidewind, U. Kaiser, J. Biskupek, F. Schmidl, and P. Seidel, Texture and electrical dynamics of micrometer and submicrometer bridges in misaligned $Tl_2Ba_2CaCu_2O_8$ films, Phys. Rev. B **70**, 104507 (2004).

[33] Yu. M. Shukrinov, A. E. Botha, S. Yu. Medvedeva, M. R. Kolahchi, and A. Irie, Structured chaos in a devil's staircase of the Josephson junction, Chaos **24**, 033115 (2014).

[34] K.-J. Lee, A. Deac, O. Redon, J.-P. Nozieres, and B. Dieny, Excitations of incoherent spin-waves due to spin-transfer torque, Nat. Mater. **3**, 877 (2004).

[35] Z. Yang, S. Zhang, and Y. C. Li, Chaotic Dynamics of Spin-Valve Oscillators, Phys. Rev. Lett. **99**, 134101 (2007).

[36] D. Laroze, J. Bragard, O. J. Suarez, and H. Pleiner, Characterization of the chaotic magnetic particle dynamics, IEEE Trans. Magn. **47**, 3032 (2011).

[37] J. Bragard, H. Pleiner, O. J. Suarez, P. Vargas, J. A. C. Gallas, and D. Laroze, Chaotic dynamics of a magnetic nanoparticle, Phys. Rev. E **84**, 037202 (2011).

[38] L. M. Pérez, J. Bragard, H. Mancini, J. A. C. Gallas, A. M. Cabanas, O. J. Suarez, and D. Laroze, Effect of anisotropies on the magnetization dynamics, Networks Heterogen. Media **10**, 209 (2015).

[39] J. A. Vélez, J. Bragard, L. M. Pérez, A. M. Cabanas, O. J. Suarez, D. Laroze, and H. L. Mancini, Periodicity characterization of the nonlinear magnetization dynamics, Chaos **30**, 093112 (2020).

[40] R. L. Kautz, Noise, chaos, and the Josephson voltage standard, Rep. Prog. Phys. **59**, 935 (1996).

[41] I. Shimada and T. Nagashima, A numerical approach to ergodic problem of dissipative dynamical systems, Prog. Theor. Phys. **61**, 1605 (1979).

[42] G. Benettin, L. Galgani, A. Giorgilli, and J. Strelcyn, Lyapunov characteristic exponents for smooth dynamical systems and for Hamiltonian systems; a method for computing all of them, Meccanica **15**, 21 (1980).

[43] A. Wolf, J. B. Swift, H. L. Swinney, and J. A. Vastano, Determining Lyapunov exponents from a time series, Phys. D (Amsterdam, Neth.) **16**, 285 (1985).

[44] N. V. Stankevich, N. A. Shchegoleva, I. R. Sataev, and A. P. Kuznetsov, Three-dimensional torus breakdown and chaos with two zero Lyapunov exponents in coupled radio-physical generators, J. Comput. Nonlinear Dynam. **15**, 111001 (2020).

[45] E. A. Grines, A. Kazakov, and I. R. Sataev, On the origin of chaotic attractors with two zero Lyapunov exponents in a system of five biharmonically coupled phase oscillators, Chaos **32**, 093105 (2022).

[46] R. Meucci, S. Euzzor, E. Pugliese, S. Zambrano, M. R. Gallas, and J. A. C. Gallas, Optimal Phase-Control Strategy for Damped-Driven Duffing Oscillators, Phys. Rev. Lett. **116**, 044101 (2016).

[47] J.-P. Eckmann, S. Oliffson Kamphorst, and D. Ruelle, Recurrence plots of dynamical systems, Europhys. Lett. **4**, 973 (1987).

[48] N. Marwan, M. C. Romano, M. Thiel, and J. Kurths, Recurrence plots for the analysis of complex systems, Phys. Rep. **438**, 237 (2007).

[49] N. Marwan and C. L. Webber, Mathematical and computational foundations of recurrence quantifications, in *Recurrence Quantification Analysis: Theory and Best Practices*, edited by C. L. Webber, Jr. and N. Marwan (Springer International Publishing, Cham, 2015), pp. 3–43.

[50] Yu. M. Shukrinov, I. R. Rahmonov, A. Janalizadeh, and M. R. Kolahchi, Anomalous Gilbert damping and Duffing features of the superconductor-ferromagnet-superconductor φ_0 Josephson junction, Phys. Rev. B **104**, 224511 (2021).

[51] G. Benettin, L. Galgani, A. Giorgilli, and J.-M. Strelcyn, Lyapunov characteristic exponents for smooth dynamical systems and for Hamiltonian systems; a method for computing all of them. Part 1, Meccanica **15**, 9 (1980).

[52] H. Haken, At least one Lyapunov exponent vanishes if the trajectory of an attractor does not contain a fixed point, Phys. Lett. A **94**, 71 (1983).

[53] J. Bragard, J. A. Vélez, J. A. Riquelme, L. M. Pérez, R. Hernández-García, R. J. Barrientos, and D. Laroze, Study of type-III intermittency in the Landau-Lifshitz-Gilbert equation, Phys. Scr. **96**, 124045 (2021).

[54] A. Janalizadeh, I. R. Rahmonov, S. A. Abdelmoneim, Yu. M. Shukrinov, and M. R. Kolahchi, Nonlinear features of the superconductor-ferromagnet-superconductor φ_0 Josephson junction in the ferromagnetic resonance region, Beilstein J. Nanotechnol. **13**, 1155 (2022).

[55] V. Paar and N. Pavin, Intermingled fractal Arnold tongues, Phys. Rev. E **57**, 1544 (1998).

[56] Y. Liu, Y. Chen, and Q. Cao, The structure of Arnold tongue overlaps in Duffing equation without small parameters, Int. J. Bifurc. Chaos. **21**, 1637 (2011).

[57] M. Nashaat, M. Sameh, A. E. Botha, K. V. Kulikov, and Yu. M. Shukrinov, Bifurcation structure and chaos in dynamics of nanomagnet coupled to Josephson junction, Chaos **32**, 093142 (2022).

[58] W. H. Press, S. A. Teukolsky, W. T. Vetterling, and B. P. Flannery, *Numerical Recipes: The Art of Scientific Computing*, 3rd ed. (Cambridge University Press, New York, 2007).

[59] M. d'Aquino, F. Capuano, G. Coppola, C. Serpico, and I. D. Mayergoyz, Efficient adaptive pseudo-symplectic numerical integration techniques for Landau-Lifshitz dynamics, AIP Adv. **8**, 056014 (2018).

[60] F. Capuano, G. Coppola, L. Rández, and L. de Luca, Explicit Runge-Kutta schemes for incompressible flow with improved energy-conservation properties, J. Comput. Phys. **328**, 86 (2017).